The quantum dynamics of H2 on Cu(111) at a surface temperature of 925 K: comparing state-of-the-art theory to state-of-the-art experiments 2

Smits, B.; Somers, M. F.

The Journal of Chemical Physics

The quantum dynamics of H_2 on Cu(111) at a surface temperature of 925 K: Comparing state-of-the-art theory to state-of-the-art experiments 2

Cite as: J. Chem. Phys. **158**, 014704 (2023); https://doi.org/10.1063/5.0134817
Submitted: 14 November 2022 • Accepted: 19 December 2022 • Accepted Manuscript Online: 20 December 2022 • Published Online: 05 January 2023

B. Smits and M. F. Somers

The Journal of Chemical Physics ARTICLE scitation.org/journal/jcp

The quantum dynamics of H_2 on Cu(111) at a surface temperature of 925 K: Comparing state-of-the-art theory to state-of-the-art experiments 2

Cite as: J. Chem. Phys. 158, 014704 (2023); doi: 10.1063/5.0134817
Submitted: 14 November 2022 • Accepted: 19 December 2022 •
Published Online: 5 January 2023

B. Smits and M. F. Somers[a)]

AFFILIATIONS

Leiden Institute of Chemistry, Leiden University, Gorlaeus Building, 2300 RA Leiden, The Netherlands

[a)]Author to whom correspondence should be addressed: m.somers@chem.leidenuniv.nl

ABSTRACT

State-of-the-art 6D quantum dynamics simulations for the dissociative chemisorption of H_2 on a thermally distorted Cu(111) surface, using the static corrugation model, were analyzed to produce several (experimentally available) observables. The expected error, especially important for lower reaction probabilities, was quantified using wavepackets on several different grids as well as two different analysis approaches to obtain more accurate results in the region where a slow reaction channel was experimentally shown to be dominant. The lowest reaction barrier sites for different thermally distorted surface slabs are shown to not just be energetically, but also geometrically, different between surface configurations, which can be used to explain several dynamical effects found when including surface temperature effects. Direct comparison of simulated time-of-flight spectra to those obtained from state-of-the-art desorption experiments showed much improved agreement compared to the perfect lattice BOSS approach. Agreement with experimental rotational and vibrational efficacies also somewhat improved when thermally excited surfaces were included in the theoretical model. Finally, we present clear quantum effects in the rotational quadrupole alignment parameters found for the lower rotationally excited states, which underlines the importance of careful quantum dynamical analyses of this system.

I. INTRODUCTION

The dissociative chemisorption of hydrogen on a Cu(111) surface has, over the years, become a model system for the field of heterogeneous gas-surface catalysis, with a wide array of available experimental[1–8] and theoretical[9–24] data. Here, the focus is on describing the elementary reaction step of the dissociation of a small molecule on a (metal) surface, which is prevalent as the chemically rate-limiting step in many industrial processes, such as the Haber–Bosch process[25] (N_2 on Fe) or methane steam reforming[26] (CH_4 on Ni). However, one of the facets not always well described by previous studies is the potential thermal distortion effect of, and energy exchange with, the surface has on these dissociation reactions.[27,28]

In our previous studies, we have demonstrated that the static corrugation model (SCM) is able to accurately include all the relevant surface temperature effects for the H_2/Cu(111) system using thermally distorted, but static, surface configurations.[17,20,23,24] Over the years, several other models with varying ranges of computational costs and degrees of overall accuracy have also been proposed to include surface temperature effects. Similar to SCM, sudden approximations have been shown to work well for CH_4 dissociation, both with a reactive force-field based approach by Busnengo and co-workers, which was used to compare perfect crystal dynamics, a static distorted surface (SDS) model, and moving surface dynamics for the dissociation of CH_4 at elevated surface temperatures at a classical level.[29–31] Jackson and co-workers also investigated surface temperature effects for the CH_4 dissociation (in reduced dimensions), not only looking at statically distorted surfaces in their "sudden" model but also including a single degree-of-freedom of the surface itself.[32,33] Furthermore, Jackson *et al.* developed a reduced density matrix (RDM)[34] approach modeling the surface as a phonon

bath, which was recently used to investigate the effects of surface temperature on methane trapping on a metal surface.[35,36]

Other approaches, not based on a sudden approximation, also exist, including the static disorder parameter by Kroes *et al.*,[37] and the effective Hartree potential by Dutta and co-workers,[38,39] as well as the more general ring polymer molecular dynamics[40,41] and high-dimensional neural network potential approaches.[18,42–44] However, to our knowledge, the SCM is the first to have been applied to rigorous 6D quantum dynamics simulations,[23,24] although reduced dimensionality studies have been performed in the past.[45]

SCM relies on the sudden approximation to describe the surface temperature effects of the H_2 dissociation reaction. It was designed to modify 6D perfect lattice potential energy surfaces (PESs) with an additional term that describes the change in potential energy of the surface in its thermally distorted configurations. Previous studies have already shown that such a static surface treatment reproduces both experiment and moving surface (quasi-)classical dynamics well, both for methane[30] and hydrogen.[23,24] Furthermore, the relative simplicity of the expressions used in SCM also allow it to be used for full 6D quantum simulations of the H_2 dissociation reaction. Here, we Monte Carlo sample different (thermally distorted) surface configurations to treat the surface degrees of freedom at a quantum dynamical sudden approximation level, which has been shown to agree very well with (quasi-)classical approaches.[46] In doing so, the associated computational cost of directly adding additional surface degrees of freedom can successfully be avoided, and the possibility arises to perform (still challenging) accurate diffractive scattering calculations at low surface temperatures. These calculations can then, in the future, be directly compared to many experiments, such as the recent state-of-the-art experiments published by Chadwick *et al.*, obtained using their molecular interferometry setup.[8,47] As it stands, SCM combined with surface configurations from molecular dynamics have only been (successfully) applied to surface temperatures of 925 K, well within the classical limit where standard molecular dynamics can be used. For low surface temperatures relevant to diffraction experiments (120 K or lower), another approach will be needed to generate the correct surface configurations adhering both to Bose–Einstein statistics and without the possibility of zero-point energy leaking due to the thermostat used.

Although SCM has so far only been applied to the H_2 on Cu(111) system, its approach is expected to be general enough to be applied to other (diatomic) molecules reacting on transition metal surfaces. It is expected to perform especially well for those systems where the sudden approximation holds and where a relatively large mass mismatch between reactant and surface and short interaction times minimizes energy exchange with the surface. While the effective three-body expression for the SCM coupling potential will work for any diatomic molecule, new expressions would be required as the number of atoms are increased. This then would be an interesting topic for future research, but not the goal of this work. The availability of a dataset, for example, from the density functional theory (DFT) calculations, which can be used to fit both the perfect lattice PES as well as the SCM coupling potential, would further reduce the workload needed to apply the SCM to other systems. Thermally distorted surface configurations can be obtained for cases well within the classical limit using a variety of force-field methods, such as the embedded atom method that we employ for this work,[20] or can be approximated using, for example, the Debye–Waller factor, as was done in the earlier SCM studies.[12]

While the previous study showed the SCM reproduces experimental dissociation probabilities well for the lower energy ranges, both at a quantum and quasi-classical level, it was also demonstrated that direct comparisons to experimentally fitted dissociation curves was difficult across the entire energy range due to the uncertainties in the available experimental data.[24] Therefore, this study will focus on several observables that we can derive from earlier results, supplemented with some additional calculations where needed. We will discuss the effect of the time-step on our final quantum dynamics (QD) simulations, especially at very low reaction probabilities, and the accuracy that is expected from the methods we employ. These results can then be used to investigate the presence or absence of an experimentally observed slow channel in more depth, which was previously left an open question due to the compromise between accuracy and computational cost that had been made. We present several 2D cuts of the PES for different thermally distorted surfaces and show how the thermal displacement of surface atoms changes not only lowest barrier heights but also their position on the 2D cut. Next, we discuss several fits to the dissociation probabilities curves that were obtained, comparing fit parameters to those obtained from the experiment. We also use these fits to obtain simulated time-of-flight spectra, which should allow for a more direct comparison of experimental associative desorption results. Finally, we present results on the effect of the internal energies of the H_2 on the dissociation reaction using both rotational and vibrational efficacies and the rotational quadrupole alignment parameter. Overall, we hope the results presented here will provide a solid dataset for future experimental and theoretical work for comparison.

II. METHODS

A. Static corrugation model

The SCM is designed to describe surface temperature effects of the dissociative chemisorption of a small molecule on a surface.[12] This is done by applying two correction terms to the perfect lattice BOSS PES: a coupling potential V_{coup}, which describes the effect of the distorted surface atoms on the incoming reactant molecule, and a strain potential V_{strain}, which describes the change of potential energy due to the distorted surface atoms interacting with each other. This can be described using

$$V_{SCM}(\vec{Q},\vec{q},\vec{q}^{\,id}) = V_{BOSS}(\vec{Q}^{\,id}(\vec{Q}),\vec{q}^{\,id}) + V_{coup}(\vec{Q},\vec{q}^{\,id},\vec{q}) + V_{strain}(\vec{q}^{\,id},\vec{q}), \quad (1)$$

where $\vec{q}$ describes the positions of all surface atoms, $\vec{q}^{\,id}$ the ideal lattice positions of all surface atoms, and $\vec{Q}$ the positions of all incoming H atoms. Finally, the positions of the reacting molecules above the ideal lattice ($\vec{Q}^{\,id}$) are obtained by scaling the non-ideal c.m. coordinates of the H_2 by the thermal expansion coefficient along the lattice vectors U and V. By scaling along the lattice vectors, we ensure that the H_2 c.m. coordinates on the thermally distorted surface correspond to the same relative coordinates on the ideal surface, as the original BOSS PES is only constructed for the H_2 coordinates related to a perfect lattice configuration.[12] In other words, by

scaling $\vec{Q}$ with the thermal expansion coefficient, we ensure that no artificial torques and forces are introduced.

For static surfaces, this description can be further simplified by neglecting the strain potential during dynamics, as it is a constant value (and therefore its derivative will always be 0). Thus, the SCM enables the inclusion of thermal lattice distortions into ideal lattice BOSS dynamics, requiring only an expression for the SCM coupling potential. Details regarding the SCM can be found elsewhere,[12,17] but briefly a switched Rydberg function was chosen as the functional form for this coupling potential, with each function parameter also linearly dependent on the distance between the hydrogen atoms, to give an effective three-body coupling potential.

We again use the distorted surface configurations from a previous study of Cu(111).[20] These configurations were generated using molecular dynamics with an embedded atom method (EAM) potential that was shown to very accurately reproduce a variety of experimental characteristics, including lattice constant, phonon dispersion curves, and thermal expansion coefficients.[20,48]

The surface atom coordinates for the ideal lattice were chosen to match those of the SRP48 corrugation reduction procedure (CRP) functional as described in Ref. 15. Here, each surface atom is placed exactly in its perfect crystal lattice position for the (111) surface of the HCP copper, with the lattice constant and interlayer distances obtained from an energy minimization. This makes it functionally different from a "0 K" surface slab, where some zero-point energy ensures not every surface atom will be exactly in its perfect, or ideal, lattice position.

B. Quantum dynamics

Additional 6D QD simulations were performed using the time-dependent wave packet (TDWP) approach to solve the time-dependent Schrödinger equation. Here, the time-independent Hamiltonian of the system $[\hat{H}(\vec{Q})]$ is described as

$$\hat{H}(\vec{Q}) = -\frac{\hbar^2}{2M}\nabla^2 - \frac{\hbar^2}{2\mu r^2}\frac{\partial^2}{\partial r^2} + \frac{1}{2\mu r^2}\hat{J}^2(\theta,\phi) + V(\vec{Q}), \quad (2)$$

with $\vec{Q}(X, Y, Z, r, \theta, \phi)$ describing the six-dimensional position vector of the H_2; M and μ, respectively, the mass and reduced mass of the hydrogen molecule; and ∇ and $\hat{J}$ the nabla and angular momentum operators (related to the c.m. coordinates X, Y, Z, and the angular coordinates theta and phi, respectively).

The 6D PES $[V(\vec{Q})]$ for our surface is described either with the SRP48 corrugation reduction procedure (CRP)[49] PES,[15,50] for the perfect lattice dynamics, or with the SCM approach, where this CRP PES is extended with the effective three-body SCM coupling potential (V_{coup}). As the surface is treated on a sudden approximation level, V_{strain} of Eq. (1) is neglected. Previous work, also comparing to classical results with a moving surface and thus implicitly including V_{strain}, has shown this approximation holds very well for the H_2 and D_2 on the Cu(111) system.[20,23]

The initial wave function $\Psi(\vec{Q}, t = 0)$ is represented as the product of a rovibrational wave function $[\psi_{v,j,m_j}(r,\theta,\phi)]$ of the H_2, a two-dimensional plane wave function $[\phi(k_0^X, k_0^Y)]$ along X and Y, and a Gaussian wave packet $[u(Z; Z_0, k_0^Z)]$ centered around a point far away from the surface,

$$\Psi(\vec{Q}, t = 0) = \psi_{v,j,m_j}(r,\theta,\phi)\phi(k_0^X, k_0^Y)u(Z; Z_0, k_0^Z). \quad (3)$$

We propagate our WPs using the split operator (SPO) method,[51]

$$\Psi(\vec{Q}; t_0 + \Delta t) = \exp\left(-\frac{i}{2}K\Delta t\right)\exp(-iV(\vec{Q})\Delta t) \times \exp\left(-\frac{i}{2}K\Delta t\right)\Psi(\vec{Q}; t_0) + O[(\Delta t)^3], \quad (4)$$

with K being the kinetic energy part of our Hamiltonian, as implemented in our in-house code.[46] Here, the WPs are propagated in a stepwise fashion, first taking a half-step for the free particle propagation, then a full action of the potential is applied, followed by another half-step as a free particle. This stepwise propagation method inherently results in an error $O[(\Delta t)^3]$ that scales with the size of the time-step used.

We use a quadratic form of the optical potentials in the scattering and reactive channel regions,[52] while the scattered fraction is analyzed through the scattering matrix formalism,[53] which yields the scattering probabilities for each rovibrational state and diffraction channel separately. The sticking probability is subsequently calculated by subtracting the sum of all these scattering probabilities from the total possible probability of one. For some simulations, these sticking probabilities are also compared to those obtained from a flux analysis in r, which directly measures the flux through a plane for a specific large enough value of r, but does not yield any information on the scattered states. For a more in-depth discussion of the basis of these quantum mechanical methods, we direct the reader to Refs. 46 and 54.

Only those thermally distorted surface atoms in the top two layers of the surface slab, and within the SCM cutoff distance of 16 bohrs of the 1 × 1 unit cell corner, are included in the SCM, as this is where the coupling potential is available.[17] To obtain a single representative dissociation curve for H_2 reacting with thermally distorted Cu(111) at a QD level, we average the probabilities obtained for a total of 104 unique thermally distorted surface slabs.

As the reactive scattering of the H_2 is fast compared to the motion of the surface atoms, and the mass mismatch between the H and Cu atoms is very large, the hydrogen molecule and the solid represent two (thermally) separate systems, with the solid equilibrated to the surface temperature of 925 K, but the H_2 not. Thus, the effects of the (quantum) dynamics of the surface on the reactive scattering of the H_2 can be (implicitly) included by using the sudden approximation, Monte Carlo sampling many different surface degrees-of-freedom associated with the ≈70 surface atoms included in a typical SCM potential evaluation.

Compared to purely classical dynamics, the QD-SCM does not suffer from an incorrect redistribution of internal energies of both the solid and the hydrogen (especially when including a thermostat), or for erroneous use of Maxwell–Boltzmann statistics for the surface atoms at lower temperatures. On the other hand, the large amount of surface atoms that can be included with the SCM also provide a clear advantage over other approximate quantum dynamical studies, which generally make use of reduced degrees-of-freedom of the solid,[14,23] or describe the dynamics of the surface using a few Hartree

products as ansatz.[38,39] Furthermore, with no need for a harmonic oscillator approximation for the surface, the SCM allows for thermal expansion effects of the solid to be included, which have been shown to be clearly of relevance.[12]

Especially, for the SCM and low surface temperatures, one could use (with the proper periodic boundary conditions and using the quasi-harmonic approximation[55]) the phonon displacement vectors to sample surface configurations with the correct Bose–Einstein statistics. This then allows for a more direct comparison to earlier[56] and more recent state-of-the-art diffraction experiments[8,47] using a full quantum description of both H_2 and the solid, albeit within the sudden approximation where energy exchange is not taken into account.

We expand on the available QD results of the previous study by adding a WP in the 0.95–1.50 eV energy range for the results in the initial vibrational ground state. Also included is the WP in the 0.65–1.00 eV range for the $v = 1$ and $J = 1$ states. For the initially rotationally excited states, only those states with $m_J \geq 0$ were considered, with the results for $m_J \neq 0$ counted twice in the total average per rotational state to account for the $m_J < 0$ states. The results in the 0.10–0.30 and 0.25–0.70 eV range are taken from a previous study (Ref. 23). Details regarding the computational parameters for each of these wave packets can be found in the supplementary material.

C. Quasi-classical dynamics

Quasi-classical trajectories are performed by propagating the H_2 molecules in the microcanonical ensemble with the Bulirsch–Stoer predictor–corrector algorithm.[57] Again, we use the SRP48 CRP, perfect lattice, PES,[15,50] or the extended SCM PES for one of the statically distorted surfaces. Propagation ends when the Z c.m. coordinate is more than 7 Å from the surface for a scattered trajectory or when the two H atoms move more than 2.25 Å apart for a reactive trajectory. Propagation is also stopped after 20 ps, with the H_2 considered trapped if it has not either dissociated or scattered yet, although this does not generally occur for the H_2/Cu(111) system.

The initial configurations of the c.m. of the H_2 is randomly selected along the lattice vectors $U(= X - Y/\sqrt{3})$ and $V(= 2Y/\sqrt{3})$ with a value between 0 and the lattice constant a, at a distance of 7 Å above the surface in Z. The molecular angles θ and ϕ are randomly chosen from a uniform distribution on the sphere, with $\cos(\theta)$ ranging from −1 to 1 and ϕ from 0 to 2π, respectively.

To expand to *quasi*-classical dynamics, the initial rovibrational state is quantized and a zero-point energy is added, which has been shown to increase accuracy of classical simulations for H_2 on metal surfaces.[46] The rovibrational energies are calculated using the Fourier grid Hamiltonian (FGH) method,[58] while a constant time-step propagation for one full vibrational cycle is performed to obtain the quasi-classical distribution of the H–H distances and the corresponding momenta. Internal angular velocities are chosen according to the quantized angular momentum $L^2 = J(J+1)\hbar^2$, while the angle θ_L between the angular momentum vector and the surface normal is chosen randomly but constrained by $\theta_L = \pi$ for $J = 0$ and $\cos(\theta_L) = m_J/\sqrt{J(J+1)}$ for $J \neq 0$. The rotational m_J states are chosen equally between $-J$ and J, with the number of trajectories increased to ensure each m_J state has the same number of occurrences.

For each trajectory performed using the SCM approach, a random surface configuration is chosen from the same dataset of 25.000 surface configurations as is used for the QD.[20] Similar to the QD PES, we include only distorted surface atoms within the SCM cutoff distance of 16 bohrs, and within the top two layers of the surface slab when calculating the SCM coupling potential, as was done in all previous studies.[20,23,24] At least 50 000 trajectories were performed for every normal incidence energy.

D. Rotational quadrupole alignment parameter

The rotational quadrupole alignment parameter $[A_0^{(2)}]$ is a measure of preference for the H_2 to dissociate, in particular, m_J states. When it is positive, dissociating molecules preferred to react with their bond axis parallel to the surface ($|m_J| = J$; "helicopter"), while negative values indicate a preference for reaction of molecules with an end-on rotation ($|m_J| = 0$; "cartwheel"). A value of 0 indicates no preference for either.

It is defined as

$$A_0^{(2)} \equiv \langle 3\cos^2\theta_L - 1 \rangle, \tag{5}$$

with θ_L the angle between the angular momentum vector and the surface normal. It can also be computed through

$$A_0^{(2)}(v,J) = \frac{\sum_{m_J} P_{stick}(v,J,m_J)\left(\frac{3m_J^2}{J(J+1)} - 1\right)}{\sum_{m_J} P_{stick}(v,J,m_J)}, \tag{6}$$

with $P_{stick}(v,J,m_J)$ the sticking probabilities for the specific rovibrational state. Assuming direct inversion under detailed balance, it can also be measured experimentally, although there are no studies available for the H_2 on Cu(111) system to our knowledge; however, some data for D_2 are available.[5,59,60]

E. Simulating time-of-flight spectra

To more directly compare the time-of-flight (ToF) spectra obtained from the state-selective desorption experiments, we can also directly simulate ToF spectra from our dissociation curves. Mirroring the experimental approach as described in Ref. 2, we make use of direct inversion under detailed balance to directly relate the dissociative adsorption results to the ToF spectra of associative desorption results. Here, we relate the intensity of the ToF spectrum to the sticking probability function multiplied by a flux-weighted velocity distribution expressed in the time domain, accounting for the $\frac{t'}{x_0}$ term due to the detection method used,

$$I(t')dt' = K \cdot C(t') \cdot \exp\left(\frac{-E_{kin}[t']}{2k_b T_s}\right)\left(\frac{x_0}{t'}\right)^4 \cdot P_{stick}(E_{kin}[t'])\, dt', \tag{7}$$

with k_b the Boltzmann constant, T_s the surface temperature, K a proportionality constant, $E_{kin} = m\left(\frac{x_0}{t'}\right)^2$, and $t' = t - t_{shift}$. A cutoff function $[C(t')]$ is also included, which models the experimental decrease in ion detection efficiency as kinetic energy decreases.[7] Here, t, (t_{shift}), and x_0 describe the travel time in (after leaving) the field-free region, and the length of this field-free region in the detector of the experimental setup that is being simulated, respectively. Using this expression, the assumption is made that all molecules

desorb parallel to the surface normal, completely neglecting any off-normal contribution to the final signal, which means we can set the kinetic energy E_{kin} equal to the kinetic energy normal to the surface E_n. While more complicated expression do exist that can take this additional factor into account,[13] we will primarily compare it to the experimental work of Kaufmann *et al.*, where this angular averaging can be fully neglected.[7]

The cutoff function that we used was of an exponential form

$$C(E_{kin}) = 1 - e^{-E_{slope}(E_{kin}-E_{min})} \quad \text{for } E_{kin} > E_{min} \tag{8}$$

based on the kinetic energy of the molecule, as was done in the experimental study.[7] The cutoff parameters E_{slope}, which governs how fast the signal decays, and E_{min}, which determines a minimal energy the molecule needed to be experimentally detectable, were obtained from the same experimental study.

To simulate the ToF spectra using Eq. (7), we require a continuous representation of the dissociation curves $[P_{stick}(E_n)]$, which we obtained from fitting to several functional forms. The first is the error function (ERF) form

$$P_{stick}(E_n) = \frac{A}{2}\left[1 + \text{erf}\left(\frac{E_n - E_0}{W}\right)\right], \tag{9}$$

with A, E_0, and W the saturation value, energy at half saturation, and width of the curve, respectively. This symmetric sigmoidal function is one of the most used function forms for fitting dissociation curves, both for theoretical and experimental works, which ensures a large amount of data for comparison.

Next, we also tried fitting our curves to a Gompertz function (GMP)

$$P_{stick}(E_n) = A \cdot \exp\left[-\exp\left(-\frac{E_n - B}{C}\right)\right], \tag{10}$$

where A, B, and C similarly describe the saturation value, energy at half saturation, and width of the curve, respectively. This function is a special form of the generalized logistics function and is employed to model a large variety of different systems. In contrast to the ERF, the GMP has an asymmetric sigmoidal form, with a much more gradual increase toward the saturation value compared to the initial curve onset.

Finally, we have also tried a combination of Gompertz function and the general tanh function, used in previous studies, as the five-parameter function (FPC)

$$P_{stick}(E_n) = \frac{A \cdot \exp\left[-\exp\left(-\frac{E_n - B}{C}\right)\right]}{1 + \exp\left(-\frac{E_n - B_1}{C_1}\right)}. \tag{11}$$

Again, A, B, and C similarly describe the saturation value, energy at half saturation, and width of the curve, respectively, but now the two additional terms B_1 and C_1 increase the flexibility of the function at the cost of adding two additional parameters.

Both the QD and QCD results were fitted to these functional forms using a Levenberg–Marquardt routine, minimizing the residual difference between the available data-points and the model. For those QD results where there is an overlap between the different WPs at the same energy, the WP reaching up to higher energy was always chosen.

F. Threshold offset and efficacies

Using our state-selective results, we can also obtain both rotational and vibrational efficacies. These, in particular, indicate the ability of rotational and vibrational energy of the H_2 to promote reaction with the surface, which is an often experimentally available observable.

To best obtain these values, we make use of the method by Shuai *et al.* by first finding the energy offset between the rotational or vibrational ground state and each specific curve.[61] This "threshold offset" ΔS should allow for an analysis of the results independent of the functional form chosen, and it can also be fit directly to the sticking probability curves obtained from our dynamics and gives us another observable that we can compare to the experimental values. Again, we will make use of the Levenberg–Marquardt routine for fitting, minimizing the difference between the sticking curve of the rovibrationally excited state and the rovibrational ground state. To have a focus on the curve onset of these results, we also tried using the logarithm of both reaction curves and minimizing the difference between the two, but this did not appear to change our results significantly.

With this offset, we can then directly calculate the rotational

$$\mu_{rot}(v,J) = \frac{\Delta S(v,J) - \Delta S(v,0)}{E_{int}(v,J) - E_{int}(v,0)} \quad \text{for } J > 0 \tag{12}$$

and vibrational

$$\mu_{vib}(v,J) = \frac{\Delta S(v,0) - \Delta S(0,0)}{E_{int}(v,0) - E_{int}(0,0)} \quad \text{for } v > 0 \tag{13}$$

efficacies for our H_2/Cu(111) results. The internal energies of the molecule were obtained from the FGH method.

III. RESULTS AND DISCUSSION

A. Effect of QD timestep

In our previous study, we discuss an unphysical "upturn" present for the QD results at very low reaction and energy. While this upturn does appear within the same range as the experimental "slow"-channel fitted by Kaufmann *et al.*, its shape led us to believe it was more likely to be noise due to the split-operator method [Eq. (4)], which has an inherent error scaling with $O(\Delta t^3)$. Other parameters of the QD calculation, such as the size of the specular and scattering grid, the distance of the analysis plane from the optical potential, and the parameters governing the optimal absorption of these optical potentials, were found to have little to no effect on the magnitude of this noise.

To verify the upturn found in the previous study and investigate the influence of the propagation timestep, we now compare our previous results to a new QD WP with a timestep of 0.1 atu (vs 1.5 atu for our original calculations), as is shown in Fig. 1. Next to these small timestep (blue) and larger timestep (orange) curves, we also include the QCD-BOSS results in black and the results of the flux analysis method on the same system and a timestep for propagation of 2.0 atu.

Comparing the obtained reaction probabilities on both the regular (a) and logarithmic (b) scale, we clearly see this "upturn" for the larger timestep results obtained with the scattering matrix (S-matrix) formalism, resulting in an error in the range of 10^{-3}. In contrast, the

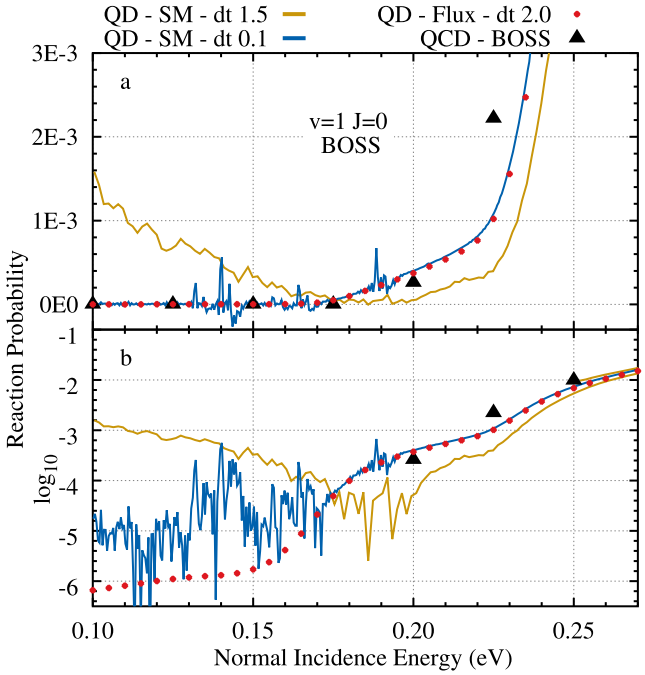

FIG. 1. Dissociative chemisorption probabilities of H_2 on Cu(111) for the first vibrationally excited state obtained using the BOSS approach and several different WPs. Included are (orange) QD results for a timestep of 1.5 atu using the S-matrix formalism, (blue) QD results for a timestep of 0.1 atu using the S-matrix formalism, (red circles) QD results for a timestep of 2.0 atu using flux analysis method, and (black triangle) QCD results. Both a regular (a) and a logarithmic (b) scale are used for the reaction probabilities.

flux analysis method appears to converge to much smaller probabilities in the 10^{-6} range, even with a larger timestep for propagation. It should, however, be noted this analysis method only yields reaction probabilities and is thus not suitable to obtain rotational and vibrational (in)elastic scattering probabilities we intend to investigate. Finally, by much reducing the timestep, we are able to reduce our error in the results of the scattering matrix formalism to the range of 10^{-5}, as can be seen by the blue curve. Interestingly, this smaller time step also has some effect on the higher energy ranges just above the threshold for reaction, slightly reducing the reaction probabilities we find similarly to how they are increased at low energy. The good agreement between flux analysis and S-matrix results does appear to indicate we obtain accurate reaction probabilities to as low as $10^{-4.5}$ (around 0.17 eV of incidence energy) where the flux analysis and S-matrix methods diverge.

Overall, these results once again underline the importance of carefully crafted wavepackets when using the TDWP approach to QD, but also give us a range of error we can expect when further analyzing the results for this and previous studies. Clearly, as in every computational study, one always needs to balance accuracy and computational cost as reducing the timestep from 1.5 to 0.1 atu makes every single WP calculation of the 104 we need to perform per energy range when including the SCM, 15 times more expensive. Such a study would thus be more than 1500 times more expensive than a traditional 6D BOSS QD WP calculation, which nowadays takes roughly 24 h on a modern 32 core CPU. Nonetheless it is noted that for probabilities at the threshold and beyond, the usual accuracy of 10^{-3} using dt = 1.5 atu is quite sufficient.

B. Barrier shape and location

Before we continue with the parameters that were derived from (fitting to) the dissociation curves obtained using QD and QCD simulations, we will first discuss several cuts of the PES and the location of the transition state found there, both for thermally distorted surfaces and the perfect crystal. These cuts will shed some light not only on the changes in lowest barrier heights brought about by including the SCM but also demonstrate how the location of the barrier can change as the surface atoms are shifted from their ideal lattice positions. These slabs were obtained from the dataset of surfaces generated in Ref. 20, through molecular dynamics at a surface temperature of 925 K, applying a highly accurate EAM potential capable of reproducing experimental lattice constants and phonon dispersion curves.[48] In Figs. 2 and 3, we present a collection of two sets of contour plots (or elbow plots) of the PES at the (lowest barrier) bridge-to-hollow (bth), and one of the top-to-fcc (ttf) reaction sites, respectively. Generally, these lowest barrier sites will have major effects on the shape of the dissociation curves, as they provide a predictive tool for the onset of the reaction. In (b), (c), and (d), we show the potential for a specific non-reactive, very reactive, and typically reactive surface slabs, respectively, while the transition state location

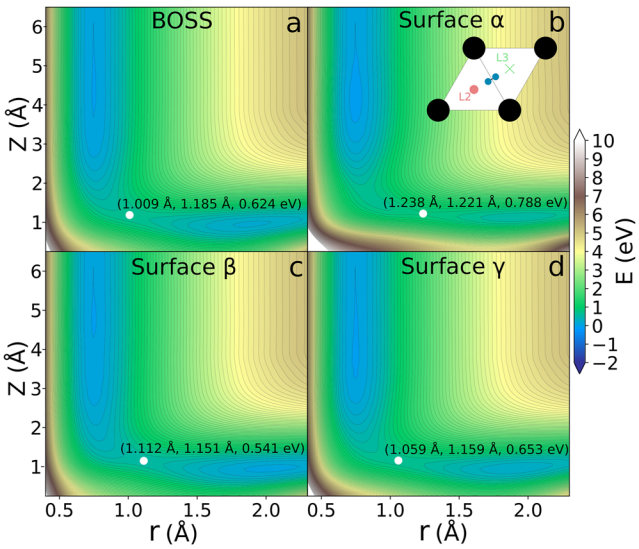

FIG. 2. Potential energy contour plot for the bridge-to-hollow (bth) reaction site, as depicted in the top right corner. The PES was fit using the CRP[49] using DFT obtained with the SRP48 functional.[15,50] Included are the potential for the (a) BOSS approach, as well as three different SCM distorted surfaces: (b) non-reactive α, (c) very reactive β, and (d) typical reactivity γ, which have also been discussed in a previous study.[23] The transition state for each 2D PES is marked with a white circle, including the location of the barrier in the (r, Z, V) format. The distorted surface slabs for the SCM, at a modeled surface temperature of 925 K, were obtained from Ref. 20.

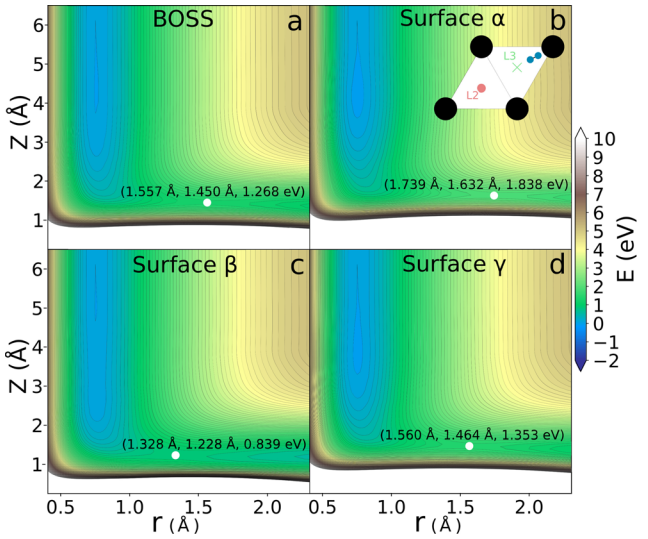

FIG. 3. Potential energy contour plot for the top-to-fcc (ttf) reaction site, as depicted in the top right corner. The PES was fit using the CRP,[49] using DFT obtained with the SRP48 functional.[15,50] Included are the potential for the (a) BOSS approach, as well as three different SCM distorted surfaces: (b) non-reactive α, (c) very reactive β, and (d) typical reactivity γ, which have also been discussed in a previous study.[23] The transition state for each 2D PES is marked with a white circle, including the location of the barrier in the (r, Z, V) format. The distorted surface slabs for the SCM, at a modeled surface temperature of 925 K, were obtained from Ref. 20.

is also marked in the (r, Z, V) format for each of these cuts. The ttf reaction site was included specifically due to its large difference in barrier between the surface slabs we discuss. These same three surface slabs have also previously been discussed in Ref. 23, where their reaction and (rovibrationally elastic) scattering probabilities were shown.

Of particular note is the shift of the lowest reaction barrier, both in r and in Z, when the surface is thermally displaced, which can have further dynamical effects also on the contribution of rovibrational energies to the dissociation reaction, as we will show in the next sections. While previous studies already carefully characterized the effect of individual surface atom displacements, both parallel and normal to the surface, on the barrier height and location,[11,14] we now also show how all these effects work together to form a very different potential energy landscape between different thermally distorted surfaces. For the (lowest barrier) bth PES cuts (Fig. 2), we find that the inclusion of surface temperature effects shifts the location of the reaction barrier toward higher H–H distances, while also slightly moving this barrier closer toward the surface. In contrast, for the lowest reaction barriers of the ttf PES cuts (Fig. 3), we find barriers with much lower (higher) r and Z values for the very reactive (non-reactive) surface slab we included. However, even the most reactive barrier here is much higher than the barriers found for the bth site and is thus more important for higher ends of the dissociation curves. We would, however, also note that this is only a very small part of the dataset of 25 000 distorted surface configurations used in this work, as each distorted surface slab will have a uniquely shaped potential energy landscape.

C. Time-of-flight spectra and fitted parameters

To get a more direct comparison to the available results of associative desorption experiments, we have simulated time-of-flight spectra for each of our dissociation curves. Here, we rely on detailed balance and several parameters of the experimental setup by Kaufmann *et al.* to allow for the best possible comparisons to their results. As the experimental setup was recalibrated every day between measurements, we chose a constant time offset (t_{shift} = 3.2 μs) and the length of the field-free region (x_0 = 29.25 mm) for Eq. (7), as was reported in Ref. 7. For the continuous expression of the dissociation curve, we use the GMP for the v = 0 QD-BOSS and all QD-SCM results, and the FPC for the v = 1 QD-BOSS and all QCD results.

As advised by the experimentalists, it was also decided to simulate the experimental ToF spectra from their ERF fits using the reported fitting parameters, as this would allow for a more direct comparison to the theoretical results. Equation (8) was used for the simulation of both the experimental and the theoretical spectra, with E_{slope} = 22.8 eV^{-1} and E_{min} = 7.2 meV as a reported typical value by Kaufmann *et al.*[7] Finally, we used a modeled surface temperature of 923 and 925 K for the experimental and theoretical results, respectively. Although using only an average of the ToF simulation parameters reduces our ability to directly compare the experimental results as they were recorded, we believe it will also reduce the error we can expect due to the needed daily calibrations. Similarly, we expect little data to be lost by simulating the experimental spectra from the ERF fits, as they have been shown to be very accurate by the experimentalists.[7]

In Fig. 4, we present the simulated ToF spectra for several rovibrational states, both for QD- and QCD-SCM and -BOSS results, compared to the simulated experimental results of Kaufmann *et al.* Of note is the broadening of the SCM results when compared to the BOSS spectra, which we attribute to the characteristic curve broadening effect due to surface temperature.[62] Here, the lower reaction barrier of some surface configurations improves dissociation, while unfavorable configurations reduce reactivity at higher energies. Peak locations found for the SCM are similarly found at a slightly longer ToF compared to the BOSS. We also find good agreement between the QD and QCD results, although some differences are found for the vibrationally excited states, similar to what is observed for the dissociation curves themselves.[24] In general, the SCM does increase agreement with the experimental spectra for all states, although it appears to perform much better for the vibrational ground states. For the rovibrationally excited states, the SCM appears to somewhat overestimate the curve broadness.

The theoretical dissociation curves were also fitted to the ERF as presented in Eq. (9), with the three fitting parameters for the QD- and QCD-SCM and -BOSS fits presented in Fig. 5 and compared to those obtained from experiment. Errorbars are included with a width of 2σ. While these fits are commonly used to efficiently compare dissociation curves, we also find the ERF functional form performs the worst, of the functional forms we tried, in accurately describing our obtained results from the QD and QCD (see the supplementary material). Nevertheless, some information can be gained by comparing these fitted parameters directly. Experimental saturation values (A) were not included, as they cannot be directly obtained from the desorption experiments, while the experimental

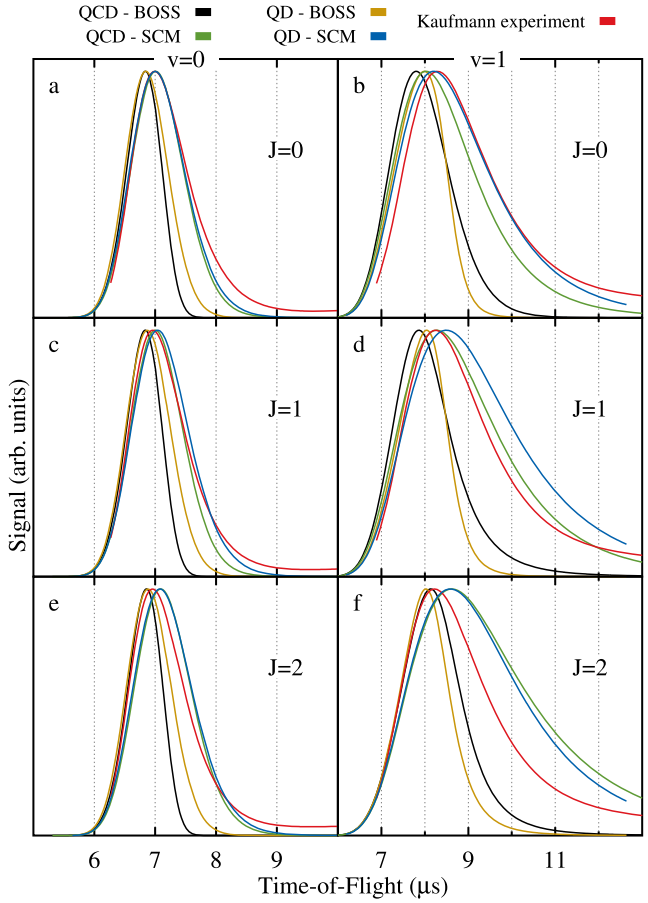

FIG. 4. Simulated time-of-flight spectra for six rovibrational states: $v = 0$ [(a), (c), and (e)] $J = 0$, 1, 2 and $v = 1$ [(b), (d), and (f)] $J = 0$, 1, 2. Spectra are generated using fits to the QD-SCM (blue), QCD-SCM (green), QD-BOSS (orange), and QCD-BOSS (black) dissociation curves, a part of which was published in Ref. 24, and fit to the GMP or FPC sigmoidal functions. Also included are the experimental results by Kaufmann *et al.*,[7] simulated using the published ERF function fits including the slow channel. A surface temperature of 925 and 923 K was used for the theoretical and experimental simulations, respectively.

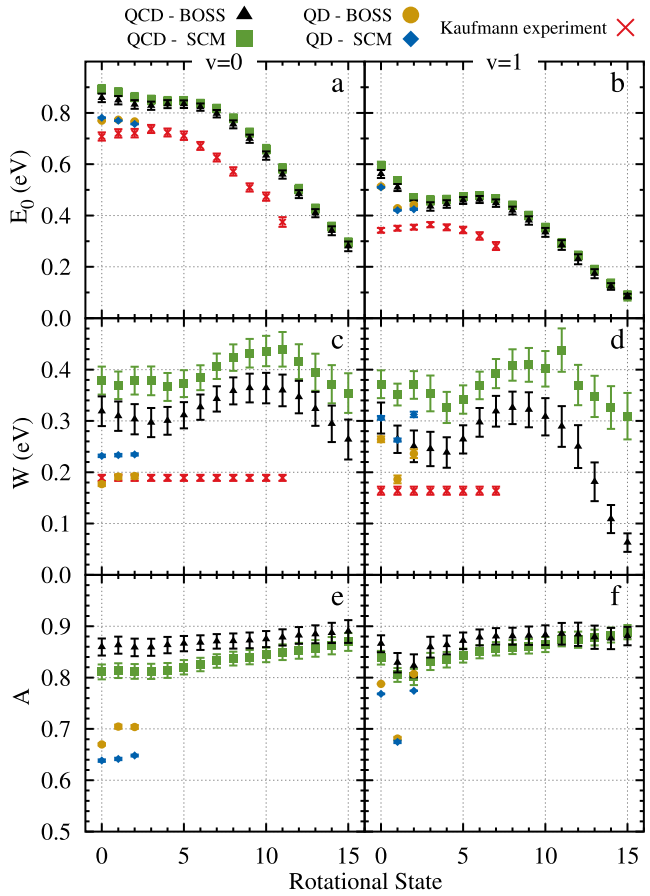

FIG. 5. Fitted ERF parameters for the fits to the QD-SCM (blue), QCD-SCM (green), QD-BOSS (orange), and QCD-BOSS (black) dissociation curves, for the [(a), (c), and (e)] $v = 0$ and [(b), (d), and (f)] $v = 1$ vibrational states, plotted against the rotational (J) state. Included are the [(a) and (b)] E_0, [(c) and (d)] W, and [(e) and (f)] A parameters, as shown in Eq. (9). Where available, the experimental results of Kaufmann *et al.*[7] are also included. Errorbars represent a standard deviation of 2σ, obtained from the fitting procedure.

width parameters (W) were only reported as a constant value per vibrational state.

We observe a slight difference between the E_0 parameters [Figs. 5(a) and 5(b)] of the BOSS or SCM approaches, both at a QD and QCD level. Those parameters found when fitting the QD results are however somewhat lower in energy, more so for the vibrational ground state (a) than the vibrationally excited state (b). The experimental fits yielded even lower values, although qualitatively theory appears to generally predict the right shape as the rotational state increases, where reaction occurs earlier as the rotational energy increases. Only at the lowest rotational states do we see small qualitative differences, where the experiment predicts a small increase in E_0, which theory only finds later around $J = 5$.

For the curve widths (W) [Figs. 5(c) and 5(d)], we see a similar split between experiment and theory, where both the SCM and BOSS predict higher widths than found for the experimental fits. Both the QD- and QCD-SCM results show a higher curve width than the matching QD- and QCD-BOSS results, as is characteristic for surface temperature effects. Focusing on the QCD widths, we see that they generally very slowly decrease as the rotational state increases, which we can attribute to the additional rotational energy helping the molecule pass the barrier without opening up new reaction paths at higher barriers. At higher rotation, the new increase in width could indicate the opening up of later (in r) reaction pathways, which are more efficiently surpassed for molecules with a higher rotational state. This can be understood by the scaling of $\frac{1}{r^2}$ as found in Eq. (2): as r increases, the rotational energy of the molecule must decrease to ensure conservation of angular momentum as it approaches the barrier and does not change state. This rotational energy can then thus assist in surpassing the dissociation barrier.[63] Finally, at very high J-states, even these latter barriers are easily passed by the very high (rotational) energy of the molecule,

and widths rapidly decrease again. Especially for the vibrationally excited states, this decrease is likely due to the internal energy of the molecule being high enough to allow for the dissociation to occur, even without any significant kinetic energy towards the surface.

It is known that for H_2 on Cu, the vibrational energy can assist in promoting the reaction, which we also discuss in Sec. III D. Somewhat similar effects were observed in one of the earliest studies using the SCM; however, here the decrease in width for the higher (rotational) states was much less apparent.[12] Unfortunately, not enough rotational states have been calculated to attempt a similar analysis for the QD results, and similarly, the experimental results were only fitted to a single width per vibrational state.

For the saturation values (A) [Figs. 5(e) and 5(f)], we find that the BOSS approach generally predicts slightly higher values than the SCM, although this difference decreases as the internal energy of the molecule increases. This can be well explained by a change in barrier heights, locations, and/or the potential energy landscape surrounding these barriers, when considering different surface configurations, which we show to have a major effect (see Sec. III B). Here, some non-reactive configurations will simply have no clear reaction path on some higher barrier regions of the full potential. These specific surface slabs would then be much less reactive, decreasing the maximum reaction probabilities that are obtained when sampling many configurations.

A also increases very slowly as the internal energy goes up, which can be explained easily by even the highest reaction barriers being more easily overcome in the incidence energy ranges we investigated. The values for the (QCD-)SCM approach increase slightly faster, likely due to the much larger collection of different barriers available due to all the different surface configurations. One clear dip in saturation shows the vibrationally excited states around the J = 1 and J = 2 states. It is not exactly clear if this is an expected feature, although perhaps the low rotational energy combined with the excited vibrational state prevents the molecule from easily surpassing the reaction barrier due to unfavorable rotational angles. In contrast, for the rotational ground state, there would be no (significant) rotation to have any effect, while for higher states, the much higher rotational energy can more easily facilitate reaction purely energetically.

QD results predict a lower saturation than those obtained with QCD, with slightly closer to those predicted by some experimental studies, although it is unclear what could cause this difference. It could be simply related to the fact that energy can be far more easily converted between degrees of freedom in QCD, when compared to QD, where the molecule cannot as easily convert its internal energy into degrees of freedom related to the reaction path.

D. Rotational and vibrational efficacies

The "threshold offset" parameter (ΔS) will give us an indication of the increase in reaction probability due to the additional internal energy of higher rovibrational states. It is represented by the energy shift required to give the optimal overlap between the results of the rovibrational ground state and the rovibrationally excited states. As was suggested by previous studies, we can use ΔS to determine how efficiently the internal rotational [Eq. (12)] and vibrational [Eq. (13)] energies promote the dissociation reaction in a way that is more independent from the functional form chosen when fitting the dissociation curves. Indeed, we find negligible differences in ΔS when obtained from fits to different sigmoid functions (ERF, GMP, and FPC) or even using the raw results directly.

In Fig. 6, we compare the obtained offsets for the vibrational ground state (a) and vibrational excited state (b), plotted for each rovibrational internal energy (obtained from the FGH method). In contrast to experiment, we do not find small negative ΔS values for very low rotational states of the vibrational ground state. Instead, we see a rapid increase in offset value, followed by a small region of constant shift around J = 5, which is especially noticeable for the v = 1 results, as is also reflected in the similar behavior of the E_0 parameters presented in Fig. 5. For the higher internal energies, at higher rotational states, we see both the theory and experiment move toward a linear section. Interestingly, the QCD-SCM results appear to increase slightly more rapidly compared to the QCD-BOSS results, which is more obvious for the v = 1 states in Fig. 6(b). This, combined with the generally higher values for the SCM, would indicate the internal energy of the H_2 molecule can be more easily used to surpass the dissociation barrier of the thermally distorted surfaces compared to the perfect crystal lattice, which could be explained by the much more varied number of barriers encountered on the distorted surfaces, and their sensitivity to different rovibrational energies. The agreement between the QCD and QD results appears to be excellent, although little can be concluded of the shape of the full range of internal energy due to the limited amount of QD data available.

The rotational efficacies in Fig. 7 show the expected trends based on these threshold offsets. The differences between the theory and experiment, however, are much more pronounced due to the very small rotational energies involved. Therefore, we also

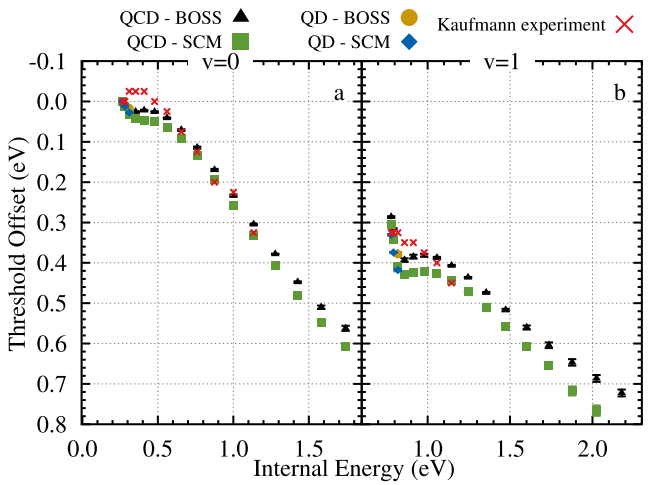

FIG. 6. Threshold offset parameters for the QD-SCM (blue), QCD-SCM (green), QD-BOSS (orange), and QCD-BOSS (black) dissociation curves for the (a) v = 0 and (b) v = 1 vibrational states, plotted against the total internal (rovibrational) energy of the H_2 molecule. Internal energies are obtained from the FGH method for the SRP48 PES. Where available, the experimental results of Kaufmann *et al.*[7] are also included. Errorbars represent a standard deviation of 2σ, obtained from the fitting procedure.

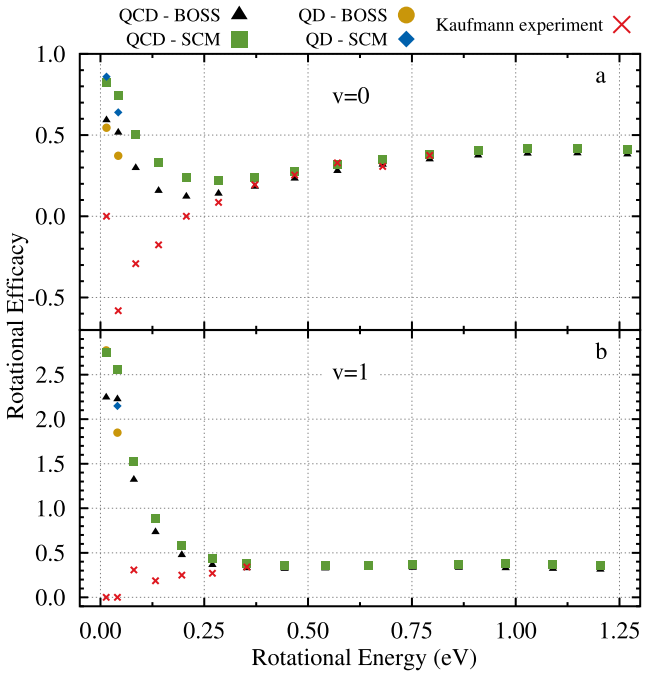

FIG. 7. Rotational efficacies obtained for the QD-SCM (blue), QCD-SCM (green), QD-BOSS (orange), and QCD-BOSS (black) dissociation curves for the (a) $v = 0$ and (b) $v = 1$ vibrational states, plotted against the rotational energy of the H_2 molecule. Rotational energies are obtained from the FGH method for the SRP48 PES, calculated using Eq. (12). Where available, the experimental results of Kaufmann *et al.*[7] are also included.

expect there to be larger errors present both in the theoretical and experimental results, although we do expect the basic trends we describe and the comparisons between the purely theoretically obtained results below to be accurate enough. For the low rotational states, experiments predict a negative efficacy, where rotation actually hinders the dissociation reaction, whereas our theory predicts a very efficient use of rotational energy to pass the reaction barrier. For the vibrationally excited states in (b), we even find efficacies above 1, which would indicate 1 meV of rotational energy would help passing over more than 1 meV of reaction barrier. This then would be well explained by very late reaction barriers, where rotational energy can greatly contribute to the dissociation reaction. QD- and QCD-SCM efficacies appear to be slightly higher than those found for BOSS, which again indicates the rotational energy can be more efficiently used to pass the barrier at low J-states and matches well with the later barriers (in r) we find in Fig. 2. Nevertheless, both SCM and BOSS, together with experiment, move toward a single efficacy value of around 0.40 at high rotational states, with the SCM values perhaps a smidgin higher still. Again, we do see an excellent good agreement between QD and QCD, but the limited amount of QD states sampled makes it difficult to draw any definitive conclusions.

The vibrational efficacies we find, as presented in Table I, agree well with each other and the experiment. The QD results are generally slightly higher than those of the QCD, opposite to what we find for μ_{rot}. However, we do again find slightly higher efficacies for the

TABLE I. Vibrational efficacies for the QD-SCM, QCD-SCM, QD-BOSS, and QCD-BOSS approaches, as well as the experimental results of Kaufmann *et al,*[7] calculated using Eq. (13).

	QD		QCD		
	BOSS	SCM	BOSS	SCM	Experiment
μ_{vib}	0.593	0.645	0.560	0.595	0.636

SCM results, compared to BOSS. Thus, our model predicts that the surface distortions allow for a more efficient use of vibrational, as well as rotational, energy to pass the dissociation barrier of the surface. This can, at least partially, be explained by the large number of different potential energy landscapes we investigate when applying the SCM and its large number of different surface configurations, although it is likely that energetic effects also play a role.

E. Rotational quadrupole alignment parameter

Finally, we will discuss another way of looking at the effect of the internal orientation of the molecule on the reaction: the rotational quadrupole alignment parameter (RQAP). This parameter describes the molecule's "preference" of reacting either initially rotating normal to the surface (cartwheel) for negative values or parallel to the surface (helicopter) for positive values, while at exactly 0 we find no preference for either. A previous study has already shown that the SCM can predict these $A_0^{(2)}$ for the D_2/Cu(111) system, although this was only checked at a QC level.[12] Similarly, previous studies have also calculated this parameter using QD methods for H_2/D_2 on perfect crystal Cu surfaces.[64,65] However, to our knowledge, RQAPs computed using both QCD and QD, including surface temperature effects, have never been compared to each other directly, especially obtained using the same potential and based on the same underlying (SRP-DFT) functional. Yet, they are of special interest for our methods, as surface temperature effects have previously been shown to clearly affect their values.[12] RQAPs, as shown in Fig. 8, were only computed for those incidence energies with a reaction probability higher than 1%, with the QD-SCM results per surface only included in the average above this same value. Especially for the QD-SCM, this greatly reduced the noise at very low energy, but did not affect the qualitative shape of the curves.

In general, we find that the QD simulations predict much higher RQAPs than the QCD results, both for the BOSS and the SCM. It is not immediately clear why these QD alignment parameters are much higher. One could argue that QCD allows for a much simpler redistribution of the internal rovibrational energies during dynamics, when compared to the QD simulations, which makes it easier to promote reaction even when the initial state is not favorable. Interestingly, in case of higher rotational states, where there are a lot more states available, this effect appears to be mostly gone. (See also the supplementary material, Fig. S6.) For these higher rotational states, no QD simulations were available for comparison.

For almost every curve, the highest alignments are not found at the lowest energy we include, instead only slightly behind these lowest barriers. This would then imply at least some of the lowest

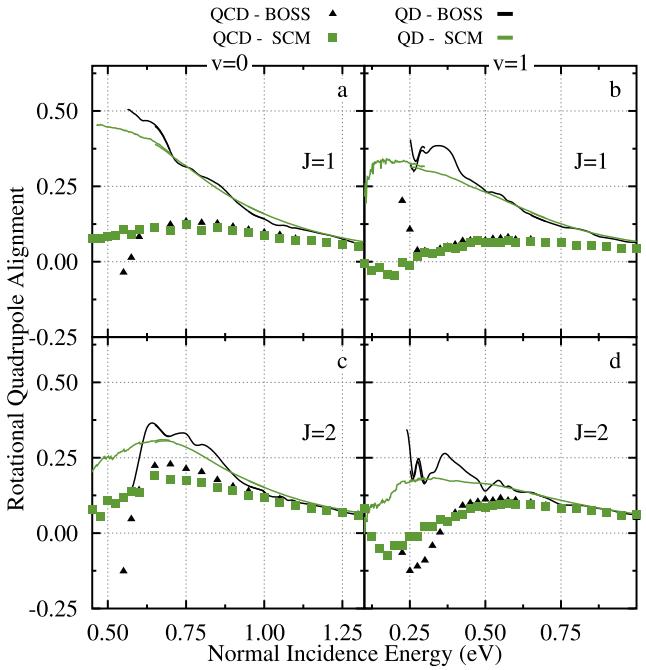

FIG. 8. Rotational quadrupole alignment parameters obtained for the SCM (green curves and squares) and the BOSS (black curves and triangles) approaches for the $v = 0$; $J = 1$, $J = 2$ [(a) and (c)] and the $v = 1$; $J = 1$, $J = 2$ [(b) and (d)] rovibrational states. QD results are shown as curves, while QCD results are included as symbols (squares and triangles), calculated using Eq. (6).

reaction barriers show less of a preference for rotation parallel to the surface. However, lower incidence energies also allow the molecule more time to favorably align itself to more easily surpass the reaction barriers, as the RQAPs are only determined using the initial rovibrational state in the gas phase. Furthermore, the location of the (energetically) available barriers could equally affect the amount of dynamical effects, such as rotational enhancement, that dominate for the different incidence energies. Indeed, for some rovibrational states, we even find negative RQAPs at low energy, implying a preference for more "cartwheel"-like rotation. No clear difference is found between the BOSS and SCM results at these lower rotational states, although especially the QD curves do show the BOSS to predict somewhat higher alignment parameters near the peak of the curves. This difference becomes much more apparent at higher J-states (see also the supplementary material, Fig. S6), as was observed in previous work.[12] This effect can be well explained by the distorted surface configurations modifying the reaction barriers to be less ideal for the "helicopter"-like rotation, due to, for example, "puckering" effects, where surface atoms are displaced in Z toward (or away) from the incoming reactant.

IV. CONCLUSION

We have presented our deeper analysis of the previously published 6D quantum dynamical and quasi-classical results of H_2 dissociating on a thermally distorted Cu(111) surface using the static corrugation model. As was suggested in the previous study, we show that the upturn in reaction probability we find at very low incidence energies, both for QD-BOSS and -SCM, can be entirely removed by propagating the 6D WPs with a smaller time step. Additional analysis with the flux analysis method similarly showed the upturn to not be explained by parts of the wavepackets passing past the reaction barrier in large r (H ↔H) ranges.

We show how the thermal distortion of the Cu(111) surface also leads to changes in not only the barrier height but also the barrier location and the shape of the reaction channel, when considering the H_2 dissociation, with the lowest reaction barrier moving toward slightly higher r and lower Z values.

Expanding the available QD results with several higher energy WPs, the dissociation curves obtained from theory were fitted to several sigmoidal functions. These continuous fits were then used to simulate time-of-flight spectra, where we found improved agreement between the spectra available from state-of-the-art desorption experiments and our (QD-)SCM approach when describing the H_2 dissociation reaction. The fitted parameters of the ERF sigmoidal function also showed a clear effect of curve broadening when surface temperature is included in the model, as well as small surface temperature effects. These smaller effects could be well explained by changes in both barrier height and location due to the thermal surface distortions.

Using the threshold offset parameter, which describes the energy shift required for a curve at a higher internal energy to match that of the rovibrational ground state, we compared the rotational and vibrational efficacies of our models and compared those to the values found in experiment. As expected, our theoretical results reproduced experiment well for these parameters, although the overall effect of surface temperature appeared to be very minor. Only for very low rotational energies did we find differences compared to experiment, where the rotational efficacy is predicted to be negative, which is not reproduced by any of our theoretical approaches.

Finally, we also computed rotational quadrupole alignment parameters to analyze the impact of the different rotational states on the reaction from another angle. Here, we found a much larger preference for the incoming H_2 to react with a rotation parallel to the surface when using our QD methods, compared to the QCD methods.

Overall, this work presents a wide database of experimentally obtainable parameters that can be used to validate the quality of our current and other theoretical and experimental works, when looking at the H_2 on Cu(111) dissociation reaction.

SUPPLEMENTARY MATERIAL

See the supplementary material for the computational details of the TDWP quantum dynamics simulations of H_2 dissociation on a Cu(111) surface, several figures and tables concerning the quality of the ERF, GMP, and FPC fits, as well as a selection of simulated ToF spectra and RQAPs for higher rovibrational states.

ACKNOWLEDGEMENTS

The authors thank Sven Schwabe, Daniel Auerbach, and Alec Wodtke for useful discussion regarding the experimental results and setup. The authors also thank Robert van Bree for providing

the code to generate elbow plots, and Geert-Jan Kroes and others of the theoretical chemistry group for their feedback, insights, and computational resources during this project.

AUTHOR DECLARATIONS

Conflict of Interest

The authors have no conflicts to disclose.

Author Contributions

B. Smits: Conceptualization (equal); Data curation (equal); Formal analysis (equal); Investigation (equal); Methodology (equal); Resources (equal); Software (equal); Validation (equal); Visualization (lead); Writing – original draft (lead); Writing – review & editing (equal). **M. F. Somers**: Conceptualization (equal); Data curation (equal); Formal analysis (equal); Funding acquisition (lead); Investigation (equal); Methodology (equal); Project administration (lead); Resources (equal); Software (equal); Supervision (lead); Validation (equal); Writing – original draft (supporting); Writing – review & editing (equal).

DATA AVAILABILITY

The data that support the findings of this study are available from the research group's public repository at https://pubs.tc.lic.leidenuniv.nl/.

REFERENCES

[1] H. F. Berger, M. Leisch, A. Winkler, and K. D. Rendulic, "A search for vibrational contributions to the activated adsorption of H_2 on copper," Chem. Phys. Lett. **175**, 425–428 (1990).
[2] H. A. Michelsen, C. T. Rettner, D. J. Auerbach, and R. N. Zare, "Effect of rotation on the translational and vibrational energy dependence of the dissociative adsorption of D_2 on Cu(111)," J. Chem. Phys. **98**, 8294–8307 (1993).
[3] C. T. Rettner, H. A. Michelsen, and D. J. Auerbach, "Quantum-state-specific dynamics of the dissociative adsorption and associative desorption of H_2 at a Cu(111) surface," J. Chem. Phys. **102**, 4625–4641 (1995).
[4] A. Hodgson, P. Samson, A. Wight, and C. Cottrell, "Rotational excitation and vibrational relaxation of H_2 (v = 1, J = 0) scattered from Cu(111)," Phys. Rev. Lett. **78**, 963–966 (1997).
[5] H. Hou, S. J. Gulding, C. T. Rettner, A. M. Wodtke, and D. J. Auerbach, "The stereodynamics of a gas-surface reaction," Science **277**, 80–82 (1997), publisher: American Association for the Advancement of Science Section: Report.
[6] M. J. Murphy and A. Hodgson, "Adsorption and desorption dynamics of H_2 and D_2 on Cu(111): The role of surface temperature and evidence for corrugation of the dissociation barrier," J. Chem. Phys. **108**, 4199–4211 (1998).
[7] S. Kaufmann, Q. Shuai, D. J. Auerbach, D. Schwarzer, and A. M. Wodtke, "Associative desorption of hydrogen isotopologues from copper surfaces: Characterization of two reaction mechanisms," J. Chem. Phys. **148**, 194703 (2018).
[8] H. Chadwick, M. F. Somers, A. C. Stewart, Y. Alkoby, T. J. D. Carter, D. Butkovicova, and G. Alexandrowicz, "Stopping molecular rotation using coherent ultra-low-energy magnetic manipulations," Nat. Commun. **13**, 2287 (2022).
[9] C. Díaz, E. Pijper, R. A. Olsen, H. F. Busnengo, D. J. Auerbach, and G. J. Kroes, "Chemically accurate simulation of a prototypical surface reaction: H_2 dissociation on Cu(111)," Science **326**, 832–834 (2009).
[10] C. Díaz, R. A. Olsen, D. J. Auerbach, and G. J. Kroes, "Six-dimensional dynamics study of reactive and non reactive scattering of H_2 from Cu(111) using a chemically accurate potential energy surface," Phys. Chem. Chem. Phys. **12**, 6499–6519 (2010).
[11] M. Bonfanti, C. Díaz, M. F. Somers, and G.-J. Kroes, "Hydrogen dissociation on Cu(111): The influence of lattice motion. Part I," Phys. Chem. Chem. Phys. **13**, 4552 (2011).
[12] M. Wijzenbroek and M. F. Somers, "Static surface temperature effects on the dissociation of H_2 and D_2 on Cu(111)," J. Chem. Phys. **137**, 054703 (2012).
[13] F. Nattino, A. Genova, M. Guijt, A. S. Muzas, C. Díaz, D. J. Auerbach, and G.-J. Kroes, "Dissociation and recombination of D_2 on Cu(111): *Ab initio* molecular dynamics calculations and improved analysis of desorption experiments," J. Chem. Phys. **141**, 124705 (2014).
[14] M. Bonfanti, M. F. Somers, C. Díaz, H. F. Busnengo, and G.-J. Kroes, "7D quantum dynamics of H_2 scattering from Cu(111): The accuracy of the phonon sudden approximation," Z. Phys. Chem. **227**, 130617035227002 (2013).
[15] A. Mondal, M. Wijzenbroek, M. Bonfanti, C. Díaz, and G.-J. Kroes, "Thermal lattice expansion effect on reactive scattering of H_2 from Cu(111) at T_s = 925 K," J. Phys. Chem. A **117**, 8770–8781 (2013).
[16] G.-J. Kroes, J. I. Juaristi, and M. Alducin, "Vibrational excitation of H_2 scattering from Cu(111): Effects of surface temperature and of allowing energy exchange with the surface," J. Phys. Chem. C **121**, 13617–13633 (2017).
[17] P. Spiering, M. Wijzenbroek, and M. F. Somers, "An improved static corrugation model," J. Chem. Phys. **149**, 234702 (2018).
[18] L. Zhu, Y. Zhang, L. Zhang, X. Zhou, and B. Jiang, "Unified and transferable description of dynamics of H_2 dissociative adsorption on multiple copper surfaces *via* machine learning," Phys. Chem. Chem. Phys. **22**, 13958–13964 (2020).
[19] O. Galparsoro, S. Kaufmann, D. J. Auerbach, A. Kandratsenka, and A. M. Wodtke, "First principles rates for surface chemistry employing exact transition state theory: Application to recombinative desorption of hydrogen from Cu(111)," Phys. Chem. Chem. Phys. **22**, 17532–17539 (2020).
[20] B. Smits and M. F. Somers, "Beyond the static corrugation model: Dynamic surfaces with the embedded atom method," J. Chem. Phys. **154**, 074710 (2021).
[21] E. W. F. Smeets and G.-J. Kroes, "Designing new SRP density functionals including non-local vdW-DF2 correlation for H_2 + Cu(111) and their transferability to H_2 + Ag(111), Au(111) and Pt(111)," Phys. Chem. Chem. Phys. **23**, 7875–7901 (2021).
[22] E. W. F. Smeets and G.-J. Kroes, "Performance of made simple meta-GGA functionals with rVV10 nonlocal correlation for H_2 + Cu(111), D_2 + Ag(111), H_2 + Au(111), and D_2 + Pt(111)," J. Phys. Chem. C **125**, 8993–9010 (2021).
[23] B. Smits, L. G. B. Litjens, and M. F. Somers, "Accurate description of the quantum dynamical surface temperature effects on the dissociative chemisorption of H_2 from Cu(111)," J. Chem. Phys. **156**, 214706 (2022).
[24] B. Smits and M. F. Somers, "The quantum dynamics of H_2 on Cu(111) at a surface temperature of 925 K: Comparing state-of-the-art theory to state-of-the-art experiments," J. Chem. Phys. **157**, 134704 (2022).
[25] C. Smith, A. K. Hill, and L. Torrente-Murciano, "Current and future role of Haber–Bosch ammonia in a carbon-free energy landscape," Energy Environ. Sci. **13**, 331–344 (2020).
[26] I. Chorkendorff, *Concepts of Modern Catalysis and Kinetics* (Wiley VCH, Weinheim, 2003).
[27] G.-J. Kroes and C. Díaz, "Quantum and classical dynamics of reactive scattering of H_2 from metal surfaces," Chem. Soc. Rev. **45**, 3658–3700 (2016).
[28] G.-J. Kroes, "Computational approaches to dissociative chemisorption on metals: Towards chemical accuracy," Phys. Chem. Chem. Phys. **23**, 8962–9048 (2021).
[29] Y. Xiao, W. Dong, and H. F. Busnengo, "Reactive force fields for surface chemical reactions: A case study with hydrogen dissociation on Pd surfaces," J. Chem. Phys. **132**, 014704 (2010).
[30] A. Lozano, X. J. Shen, R. Moiraghi, W. Dong, and H. F. Busnengo, "Cutting a chemical bond with demon's scissors: Mode- and bond-selective reactivity of methane on metal surfaces," Surf. Sci. **640**, 25–35 (2015).
[31] G. N. Seminara, I. F. Peludhero, W. Dong, A. E. Martínez, and H. F. Busnengo, "Molecular dynamics study of molecular and dissociative adsorption using system-specific force fields based on ab initio calculations: CO/Cu(110) and CH_4/Pt(110)," Top. Catal. **62**, 1044–1052 (2019).
[32] A. K. Tiwari, S. Nave, and B. Jackson, "The temperature dependence of methane dissociation on Ni(111) and Pt(111): Mixed quantum-classical studies of the lattice response," J. Chem. Phys. **132**, 134702 (2010).

[33]H. Guo, A. Farjamnia, and B. Jackson, "Effects of lattice motion on dissociative chemisorption: Toward a rigorous comparison of theory with molecular beam experiments," J. Phys. Chem. Lett. **7**, 4576–4584 (2016).
[34]B. Jackson, "Reduced density matrix description of gas–solid interactions: Scattering, trapping, and desorption," J. Chem. Phys. **108**, 1131–1139 (1998).
[35]B. Jackson, "The trapping of methane on Ir(111): A first-principles quantum study," J. Chem. Phys. **155**, 044705 (2021).
[36]B. Jackson, "Quantum studies of methane-metal inelastic diffraction and trapping: The variation with molecular orientation and phonon coupling," Chem. Phys. **559**, 111516 (2022).
[37]G. J. Kroes, M. Wijzenbroek, and J. R. Manson, "Possible effect of static surface disorder on diffractive scattering of H_2 from Ru(0001): Comparison between theory and experiment," J. Chem. Phys. **147**, 244705 (2017).
[38]J. Dutta, S. Mandal, S. Adhikari, P. Spiering, J. Meyer, and M. F. Somers, "Effect of surface temperature on quantum dynamics of H_2 on Cu(111) using a chemically accurate potential energy surface," J. Chem. Phys. **154**, 104103 (2021).
[39]J. Dutta, K. Naskar, S. Adhikari, J. Meyer, and M. F. Somers, "Effect of surface temperature on quantum dynamics of D_2 on Cu(111) using a chemically accurate potential energy surface," J. Chem. Phys. **157**, 194112 (2022).
[40]I. R. Craig and D. E. Manolopoulos, "Quantum statistics and classical mechanics: Real time correlation functions from ring polymer molecular dynamics," J. Chem. Phys. **121**, 3368–3373 (2004).
[41]Y. V. Suleimanov, F. J. Aoiz, and H. Guo, "Chemical reaction rate coefficients from ring polymer molecular dynamics: Theory and practical applications," J. Phys. Chem. A **120**, 8488–8502 (2016).
[42]J. Behler, "First principles neural network potentials for reactive simulations of large molecular and condensed systems," Angew. Chem., Int. Ed. **56**, 12828–12840 (2017).
[43]N. Artrith and J. Behler, "High-dimensional neural network potentials for metal surfaces: A prototype study for copper," Phys. Rev. B **85**, 045439 (2012).
[44]Q. Lin, L. Zhang, Y. Zhang, and B. Jiang, "Searching configurations in uncertainty space: Active learning of high-dimensional neural network reactive potentials," J. Chem. Theory Comput. **17**, 2691–2701 (2021).
[45]R. A. Olsen, G. J. Kroes, O. M. Lo/vvik, and E. J. Baerends, "The influence of surface motion on the direct subsurface absorption of H_2 on Pd(111)," J. Chem. Phys. **107**, 10652–10661 (1997).
[46]G.-J. Kroes and M. F. Somers, "Six-dimensional dynamics of dissociative chemisorption of H_2 on metal surfaces," J. Theor. Comput. Chem. **04**, 493–581 (2005).
[47]H. Chadwick, Y. Alkoby, J. T. Cantin, D. Lindebaum, O. Godsi, T. Maniv, and G. Alexandrowicz, "Molecular spin echoes; multiple magnetic coherences in molecule surface scattering experiments," Phys. Chem. Chem. Phys. **23**, 7673–7681 (2021).
[48]H. W. Sheng, M. J. Kramer, A. Cadien, T. Fujita, and M. W. Chen, "Highly optimized embedded-atom-method potentials for fourteen fcc metals," Phys. Rev. B **83**, 134118 (2011).
[49]H. F. Busnengo, A. Salin, and W. Dong, "Representation of the 6D potential energy surface for a diatomic molecule near a solid surface," J. Chem. Phys. **112**, 7641–7651 (2000).
[50]F. Nattino, C. Díaz, B. Jackson, and G.-J. Kroes, "Effect of surface motion on the rotational quadrupole alignment parameter of D_2 reacting on Cu(111)," Phys. Rev. Lett. **108**, 236104 (2012).
[51]M. D. Feit, J. A. Fleck, and A. Steiger, "Solution of the Schrödinger equation by a spectral method," J. Comput. Phys. **47**, 412–433 (1982).
[52]A. Vibok and G. G. Balint-Kurti, "Parametrization of complex absorbing potentials for time-dependent quantum dynamics," J. Phys. Chem. **96**, 8712–8719 (1992).
[53]G. G. Balint-Kurti, R. N. Dixon, and C. C. Marston, "Grid methods for solving the Schrödinger equation and time dependent quantum dynamics of molecular photofragmentation and reactive scattering processes," Int. Rev. Phys. Chem. **11**, 317–344 (1992).
[54]G.-J. Kroes, "Six-dimensional quantum dynamics of dissociative chemisorption of H_2 on metal surfaces," Prog. Surf. Sci. **60**, 1–85 (1999).
[55]A. Togo and I. Tanaka, "First principles phonon calculations in materials science," Scr. Mater. **108**, 1–5 (2015).
[56]D. Farias and K.-H. Rieder, "Atomic beam diffraction from solid surfaces," Rep. Prog. Phys. **61**, 1575 (1998).
[57]R. Bulirsch and J. Stoer, "Numerical treatment of ordinary differential equations by extrapolation methods," Numer. Math. **8**, 1–13 (1966).
[58]C. C. Marston and G. G. Balint-Kurti, "The Fourier grid Hamiltonian method for bound state eigenvalues and eigenfunctions," J. Chem. Phys. **91**, 3571–3576 (1989).
[59]S. J. Gulding, A. M. Wodtke, H. Hou, C. T. Rettner, H. A. Michelsen, and D. J. Auerbach, "Alignment of $D_2(v, J)$ desorbed from Cu(111): Low sensitivity of activated dissociative chemisorption to approach geometry," J. Chem. Phys. **105**, 9702–9705 (1996).
[60]D. Wetzig, M. Rutkowski, R. David, and H. Zacharias, "Rotational corrugation in associative desorption of D_2 from Cu(111)," Europhys. Lett. **36**, 31 (1996).
[61]Q. Shuai, S. Kaufmann, D. J. Auerbach, D. Schwarzer, and A. M. Wodtke, "Evidence for electron–hole pair excitation in the associative desorption of H_2 and D_2 from Au(111)," J. Phys. Chem. Lett. **8**, 1657–1663 (2017).
[62]*Dynamics of Gas-Surface Interactions*, Springer Series in Surface Sciences, edited by R. D. Muino and H. F. Busnengo (Springer-Verlag, Berlin, Heidelberg, 2013).
[63]G. R. Darling and S. Holloway, "Rotational motion and the dissociation of H_2 on Cu(111)," J. Chem. Phys. **101**, 3268–3281 (1994).
[64]J. Dai and J. C. Light, "The steric effect in a full dimensional quantum dynamics simulation for the dissociative adsorption of H_2 on Cu(111)," J. Chem. Phys. **108**, 7816–7820 (1998).
[65]E. W. F. Smeets, G. Füchsel, and G.-J. Kroes, "Quantum dynamics of dissociative chemisorption of H_2 on the stepped Cu(211) surface," J. Phys. Chem. C **123**, 23049–23063 (2019).